Geophysical Research Letters

RESEARCH LETTER
10.1029/2022GL101189

Key Points:

- We use earthquake and cross-hole experiment data at Garner Valley, CA, to monitor shear wave velocity variations in shallow materials
- The seasonal variation of shear wave velocity is up to ~25% in the top 6 m, mainly caused by pore pressure changes
- The changes of shallow seismic properties are relevant to ground motion hazard and environmental seismology

Supporting Information:

Supporting Information may be found in the online version of this article.

Correspondence to:

L. Qin and H. Qiu,
qinqiu48@gmail.com;
qiuhonrui@gmail.com

Citation:

Qin, L., Steidl, J. H., Qiu, H., Nakata, N., & Ben-Zion, Y. (2022). Monitoring seasonal shear wave velocity changes in the top 6 m at Garner Valley in southern California with borehole data. *Geophysical Research Letters*, *49*, e2022GL101189. https://doi.org/10.1029/2022GL101189

Received 9 SEP 2022
Accepted 29 NOV 2022

Author Contributions:

Conceptualization: Lei Qin, Hongrui Qiu
Data curation: Jamison H. Steidl
Formal analysis: Lei Qin, Hongrui Qiu
Funding acquisition: Jamison H. Steidl
Methodology: Lei Qin, Hongrui Qiu
Project Administration: Jamison H. Steidl, Yehuda Ben-Zion
Resources: Jamison H. Steidl, Nori Nakata, Yehuda Ben-Zion
Supervision: Yehuda Ben-Zion
Validation: Lei Qin
Writing – original draft: Lei Qin

Monitoring Seasonal Shear Wave Velocity Changes in the Top 6 m at Garner Valley in Southern California With Borehole Data

Lei Qin[1,2], Jamison H. Steidl[3], Hongrui Qiu[2], Nori Nakata[2,4], and Yehuda Ben-Zion[5,6]

[1]Hubei Subsurface Multi-scale Imaging Key Laboratory, School of Geophysics and Geomatics, China University of Geosciences, Wuhan, China, [2]Earth, Atmospheric and Planetary Sciences, Massachusetts Institute of Technology, Cambridge, MA, USA, [3]Earth Research Institute, University of California Santa Barbara, Santa Barbara, CA, USA, [4]Earth and Environmental Sciences Area, Lawrence Berkeley National Laboratory, Berkeley, CA, USA, [5]Department of Earth Sciences, University of Southern California, Los Angeles, CA, USA, [6]Southern California Earthquake Center, University of Southern California, Los Angeles, CA, USA

Abstract Subsurface structures play important roles in seismic ground motion, crustal hydrology, stability of the built environment, and more. Constraining temporal changes of subsurface shear wave velocity (V_S) can provide useful information to all these topics and the growing field of hydrological monitoring with seismic velocity. Using borehole records at Garner Valley, CA, we estimate seasonal subsurface V_S variations from impulse response functions (IRFs) of earthquake data (2005–2018) along with IRFs and cross-correlation of cross-hole experiment data (2015–2018). The inferred V_S variations are up to ~25% in the top 6 m and ~10% at 2–5 m in depth. The V_S variations correlate strongly with the water table depth changes, suggesting that the changes are mostly due to fluctuations of pore pressure in the shallow material. The shallow velocity changes alter the near-surface conditions, can affect seismic hazard estimation, and may be improperly attributed to deeper processes without careful analysis.

Plain Language Summary Seismic properties of subsurface materials are of great importance for multiple topics including surface science, estimates of seismic ground motion, and performance of considerable infrastructure. Monitoring temporal changes of seismic velocities in the top few meters provides key information for structural design and better hazard estimates. The Garner Valley Downhole Array (GVDA) is a well-instrumented test-site facility that includes seismic and pore pressure sensors installed at different depth ranges. In this study, we use seismic recordings from the GVDA to infer variations in near-surface shear wave velocity (V_S) with high spatial resolution. The results reveal significant (~25%) seasonal variations of V_S in the top 6 m that correlate well with changes in the water table. This implies that the weak near-surface soil is highly susceptible to variations in the fluid content and other loadings such as strong shaking generated by earthquakes. While the V_S variations are concentrated in the top few meters, such changes may be improperly attributed to variations of deeper structures without high-resolution data and methods.

1. Introduction

The properties and dynamics of shallow materials are of great importance for a wide range of topics including environmental seismology, seismic ground motion prediction and performance of infrastructure above and below the surface. Near-surface materials have extremely low shear wave velocities (V_S) of 100–400 m/s (e.g., Boore et al., 2011; Tanimoto & Wang, 2021; Zigone et al., 2019), and sustain variations caused by earthquakes (e.g., Nakata & Snieder, 2011; Wu et al., 2010), temperature (e.g., Oakley et al., 2021), and water level changes (e.g., Mao et al., 2022). The properties and high susceptibility to failure of shallow materials affect near-surface processes, influence the stability of vast infrastructure, alter the seismic recordings at the surface, and can mask information from deep structures (Juarez & Ben-Zion, 2020; Yang et al., 2019). Imaging properties of near-surface materials and monitoring how they respond to loadings can provide important constraints on the rheology of shallow materials with implications for seismic hazard estimates, structural engineering design, and various near-surface studies.

One critical factor that significantly influences properties of near-surface materials is the fluid content. This was investigated early on by Biot (1956a, 1956b), and examined later in laboratory experiments and with field

Writing – review & editing: Lei Qin, Jamison H. Steidl, Hongrui Qiu, Nori Nakata, Yehuda Ben-Zion

measurements (e.g., Batzle et al., 2006; Müller et al., 2010; Solazzi et al., 2019). At low saturation (usually <10%) when the effect of capillary pressure governs materials' elastic moduli, V_S increases significantly relative to dry soil, because the material strength increases due to the suction between particles (Kuster & Toksöz, 1974; Lu & Sabatier, 2009; Nur & Simmons, 1969). As saturation level increases, V_S decreases at a lower rate caused by the decrease of effective stress (De Landro et al., 2022; Dong & Lu, 2016; Qiu et al., 2015). Seismic velocities of saturated materials have been monitored to predict potential liquefaction effects (Steidl et al., 2014; Uyanik et al., 2013), infer porous media properties (Berryman et al., 2002; Cheng & Toksöz, 1979) and manage underground water resources (Clements & Denolle, 2018; Lecocq et al., 2017). However, there have been a few in situ studies of how near-surface V_S and fluids co-evolve on a decadal long term.

The Garner Valley Downhole Array (GVDA) is a well-instrumented geotechnical test-site facility, and has been providing data and analysis results for three decades now (e.g., Archuleta et al., 1992; Chandra et al., 2015; Steidl et al., 1996). The top 18 m at the site exhibits V_S between 90 and 400 m/s and Q values of 10–15 and the water table at the site depends on rainfall and seasons with depth variations up to 3 m (Bonilla et al., 2002). The instrumentation includes accelerometers installed at different depths augmented by various pore pressure transducers (Youd et al., 2004), and a cross-hole experiment installed in 2010 (ASTM, 2014). The data provide opportunities to monitor near-surface materials with evolving fluid content in response to various loadings with high spatio-temporal resolution. In this study, we analyze seismic and pore-pressure data from GVDA including the cross-hole experiment with a focus on how long-term changes in pore fluid pressure (due to rainfall and droughts) and the resulting water table changes affect the near-surface V_S.

2. Data and Method

Figure 1a provides a regional view of the GVDA site and data sources used in the study. Figure 1b shows the locations of accelerometers with a sampling rate of 200 samples per second (sps) and pore-pressure sensors at GVDA analyzed in this study. The cross-hole experiment includes a solenoid-powered dual-directional hammer located at 5 m depth and vertical-component seismic sensors at 2 m (stations 21 and 41) and 5 m (stations 11, 22, and 42) depths that record at 2,000 sps. The hammer source is activated in both directions once per week on Sundays at 7:30 a.m. from August 2015 to June 2019.

We use the impulse response functions (IRFs; e.g., Bonilla et al., 2019; Nakata & Snieder, 2012) from earthquake and cross-hole experiment data to infer S-wave travel times (t_S) between stations. We also use cross-correlation to analyze the travel time between different stations (Hoar, 1982) and compare results with those from the IRF analysis. The relative travel time variation dt/t is calculated using $(t–t_0)/t_0$ where t_0 is the median value of measured travel time t. Assuming $dv/v = -dt/t$, measurements of dt/t between different station pairs reveal temporal changes of V_S in the shallow materials at different depth ranges, and can provide a new level of information about dynamic soil behavior. It is also interesting to obtain P-wave velocity (V_P) variations. However, V_P is >1,200 m/s in the top 6 m, resulting in a short travel time on the order of 10^{-3} s and changes that are beyond the resolution of the data. The cross-hole experiment data has enough temporal resolution (2,000 sps), but lacks P wave signal (Section 3.2). We therefore focus on the temporal variation of V_S.

Precipitation and temperature recorded by the nearby weather station at San Jacinto, California (Figure 1a) and water table data at the GVDA site are compared to the observed dt/t. The water table depth is given by $h_w = 4.3–(P_t–P_b)/\rho g$, where P_b and P_t are the barometric pressure and the recording from the 4.3-m-deep pressure transducer, respectively, with ρ and g being the density of water and acceleration of gravity.

3. Results

3.1. Analysis of Earthquake Data

We analyze the IRFs between stations 01 (6 m) and 03 (22 m). Since the inter-station distance (<20 m) is much smaller than the event-station distance (a few kilometers), the wave propagation path is almost the same for the two stations. Considering that V_S is >3 km/s at the depth of events (e.g., Qiu et al., 2019) and <250 m/s in the top 6 m (e.g., Bonilla et al., 2002), Snell's law suggests the S-wave incident angle is <5°, so the propagation path between the two stations is near vertical, independent from earthquake locations. The two stations are chosen because both have high-quality borehole seismic data. Clear free-surface reflected S-waves are observed at the

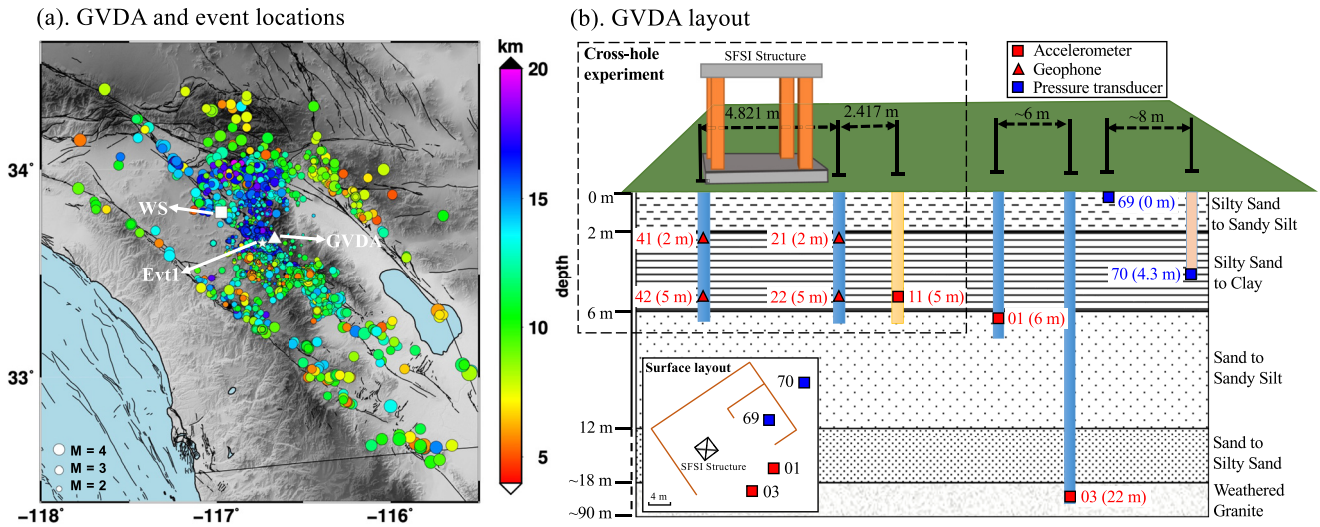

Figure 1. Array and event information: (a) Locations of the Garner Valley Downhole Array (GVDA) (white triangle), San Jacinto weather station (WS; white square), example event (Evt1; white star), and earthquakes between 2005 and 2018 that have reliable impulse response functions (color circles). (b) The configurations of GVDA. Each station is labeled with the name code and depth. Background textures represent different soil behavior types from cone penetration testing measurements, labeled on the right (http://nees.ucsb.edu/facilities/GVDA). Bottom left inset shows the surface layout. The black dashed box includes the cross-hole experiment sensors, and the hammer source is co-located with station 11. Please note that dashed lines indicate distances/depths not to scale.

6 m borehole station, and are well separated from the direct waves at the two stations. Free surface reflected S-wave is also recorded at 22 m, but does not affect the t_S measurement (Text S1 in Supporting Information S1). The measurement of two-way travel time also has a smaller relative error than measuring the one-way travel time if we use a surface sensor and borehole station 01.

We first bandpass filter the waveforms at 1–30 Hz, and calculate the IRFs via the multitaper spectral analysis (Prieto et al., 2009; Thomson, 1982) with five tapers in a 6 s time window starting 1 s before the *SH*-wave arrival. Five tapers are applied to balance the smoothness and resolution of the results. We then bandpass filter the IRFs at 1–30 Hz, normalize them by the maximum values, and interpolate from 200 to 1,000 sps to increase the time resolution of detecting peaks. Figure 2a shows the transverse-component waveforms (*SH*-waves) and IRFs from an earthquake (Evt 1 in Figure 1a). The IRF contains two prominent peaks at $t^{(1)}$ (∼0.0625 s) and $t^{(2)}$ (∼0.125 s). The parameter $t^{(1)}$ represents the travel time of direct *SH*-waves from 22 to 6 m, and $t^{(2)}$ corresponds to the *SH*-wave travel time from 22 m to the surface and then reflected downward to 6 m. We note the free surface reflection does not change the polarity of S-waves (Aki & Richards, 1980). The difference $t = t^{(2)} - t^{(1)}$ is the *SH*-wave two-way travel time in the top 6 m.

We analyze the *SH*-waves from earthquakes during 2005–2018 (Figure 1a). Events are excluded if: (1) the signal-to-noise ratio, defined as the ratio of root-mean-square values between the signal window and noise window (6-s before the *P*-wave arrival), is smaller than 2; or (2) the peak ground acceleration at GVDA is larger than 20 Gal, which may cause co-seismic V_S decrease (Qin et al., 2020). This results in ∼7,500 IRFs (Figure 2b). The primary peak at $t^{(1)}$ remains stable suggesting no significant V_S variations in the depth range 6–22 m, while the secondary peak at $t^{(2)}$ shows clear seasonal variations implying variations in the top 6 m. The travel time suggests that the average V_S is ∼250 m/s over 6–22 m, and varies between 180 and 220 m/s in the top 6 m. We track the variations of $t = t^{(2)} - t^{(1)}$ for temporal changes of V_S in the top 6 m.

We calculate the relative travel time variation *dt/t* and apply an 11-point median filter to smooth the *dt/t* curve and suppress potential *dt/t* spikes that may have been induced by earthquakes. This window size is chosen based on the tradeoff between temporal resolution and smoothness of the results. The measurement uncertainties are defined as three times the standard deviation of the difference between the raw and smoothed *dt/t* in the smoothing window. As shown in Figure 2c, the *SH*-wave *dt/t* results exhibit clear seasonal variations between −10% and 15% with an uncertainty of ±2%. Since the absolute value of *dt/t* depends on the choice of reference travel time t_0, which is the median value of *t*, we focus on the peak-to-peak amplitude of *dt/t* value that is 25%.

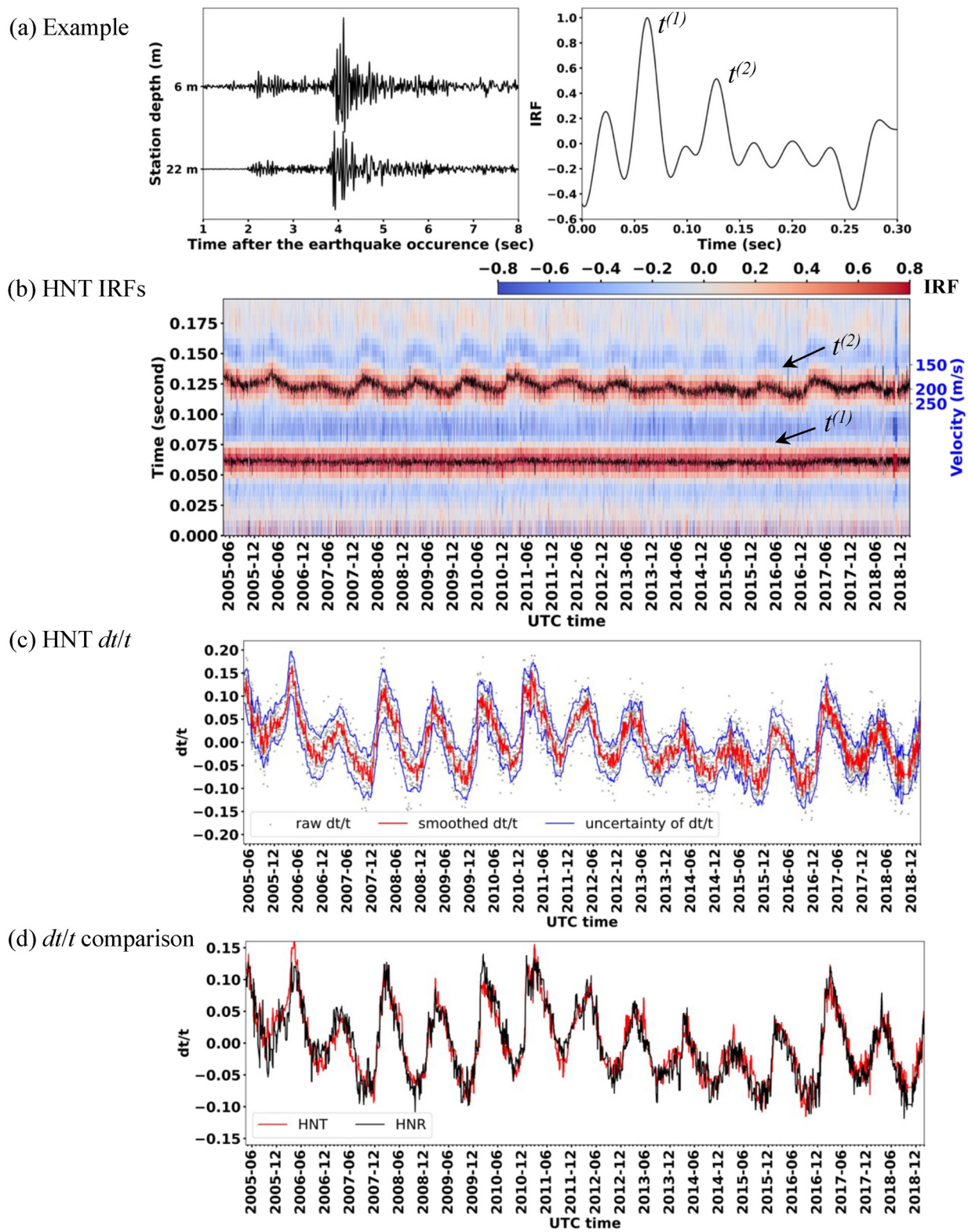

Figure 2. Earthquake data analysis: (a). Transverse-component waveforms at stations 01 (6 m) and 03 (22 m) for Evt 1 (Figure 1a) and the corresponding impulse response function (IRF). Two peaks at $t^{(1)} \approx 0.0625$ s and $t^{(2)} \approx 0.125$ s are labeled. (b). Transverse-component IRFs between stations 01 and 03 for all earthquakes. (c). Transverse-component *dt/t* before (gray dots) and after (red) smoothing. Uncertainties are outlined by blue curves. (d). Smoothed *dt/t* curves for transverse (HNT) and radial (HNR) components.

IRF results in a higher frequency band (15–30 Hz) show similar results (Figure S1 in Supporting Information S1), suggesting *dt/t* is not affected by the frequency band. We also analyze the *SV*-waves, and obtain similar IRFs (Figure S2 in Supporting Information S1), implying no significant anisotropy in the top 6 m. This is consistent with previous studies that V_S anisotropy at GVDA mainly exists in structures below 22 m due to the alignment of minerals and/or microcracks, or stress-induced pore/crack deformation (Coutant, 1996). Therefore, the estimated *dt/t* values from *SH*- and *SV*- waves are almost identical (Figure 2d).

3.2. Analysis of Cross-Hole Experiment Data

With the same method, we analyze the IRF of the cross-hole experiment data, calculated in a 0.15s-long time window centered at the arrival at station 11 (Figure 1b). The detected IRF peak amplitude provides a rough estimation of measurement quality. The velocity is obtained by dividing the distance (Table S1 in Supporting Information S1) by the travel time between the sensors, assuming straight-line propagation of S waves. Since the V_S at 5 m depth is ∼200 m/s (Bonilla et al., 2002), we interpolate the IRF from 2,000 sps to 40,000 sps, to increase the resolution of t_S estimation, and achieve a resolution of ∼0.25 m/s in detecting temporal velocity changes of V_S.

Data and IRFs from one down-swing are presented in Figure 3a. The frequency content of IRF decreases significantly with propagation distance due to geometric spreading and attenuation. This is also illustrated in the power spectral density of the data (Figure S3 in Supporting Information S1). We note the main signal's travel time is consistent with estimates from the local V_S model (Bonilla et al., 2002; Theodulidis et al., 1996), except for a slightly larger V_S value from 21-11. This suggests the vertical-component waveform is dominated by *SV*-waves, as expected for a hammer source well-coupled to the polyvinyl chloride (PVC) casing generating both *P*- and *S*-waves at the PVC/soil interface (ASTM, 2014). However, the coupling of the source to the PVC casing may generate a vertical *S*-wave line source, while we assumed a point source co-located with station 11, resulting in a slightly larger V_S value obtained from the station pair 21-11. The slightly larger V_S measurements are probably not caused by a *P*-wave signal, since the *P*- and *S*- waves are well separated based on the velocity structure and wave frequency content (Text S2 in Supporting Information S1). Therefore, this does not affect the corresponding *dt/t* measurements. Since anisotropy is not observed (Figure 2d) at the sensors' depth (2–5 m), we do not distinguish between *SV*- and *SH*- waves in the subsequent analysis.

Figure 3b presents the IRFs between stations 22 and 11 (22-11) during 2015–2019. The IRF peak amplitude indicative of the *S*-wave arrival is stable and close to 1 (colored triangles in Figure 3c), implying the S-wave is the dominating signal and the measurement of travel time is reliable. The t_S varies between 0.0102 and 0.0114 s (i.e., V_S between 235 and 218 m/s), and the *dt/t* values at 5 m depth range from −4% to 6% (orange dots in Figure 3d), resulting in 10% peak-to-peak variations. IRFs between stations 21 and 11 show similar *dt/t* variations at 2–5 m (black stars in Figure 3d), except between December 2015 and June 2016 perhaps due to the low-quality IRFs during the time period (Figure S4 in Supporting Information S1). We do not show the IRFs between stations 42/41 and 11 since they are too noisy to provide reliable *dt/t* measurements.

We also cross-correlate the data between different stations in the same time window used to calculate the IRFs (Text S2 in Supporting Information S1). The obtained t_S from 22-11 are similar to those from IRF analysis (Figure 3c), and consistent with a previous study (Hudson, 2017) that used cross-correlation between stations 22 and 42. The t_S values based on cross-correlation from other station pairs are given in Figure S5 (Supporting Information S1). Figure 3d presents the *dt/t* from different station pairs using IRFs and cross-correlations. We note that *dt/t* from station pairs 22-11, 42-11, 42-22 correspond to V_S variations at 5 m depth, while *dt/t* from 21-11, 41-11 and 41-21 represent the along-path average (i.e., between 2 and 5 m) variations between these stations. The *dt/t* at 2–5 m are similar to those at 5 m, except during December 2015 and June 2016 when low-quality data caused a spurious increase of *dt/t* with larger scatterings. We therefore conclude that the average travel time variations between 2 m and 5 m are uniform and similar to those at 5 m.

4. Discussion

Our study at GVDA indicates 25% seasonal variations of V_S over the top 6 m and 10% over the depth range 2–5 m, while little changes are observed below 6 m (Figures 2 and 3). Figure 4 compares the *dt/t* measurements with temperature and precipitation data from a nearby weather station at San Jacinto, California (Figure 1a), and the water table depth at the site. Increasing *dt/t* correlates well with increasing precipitation and rising water

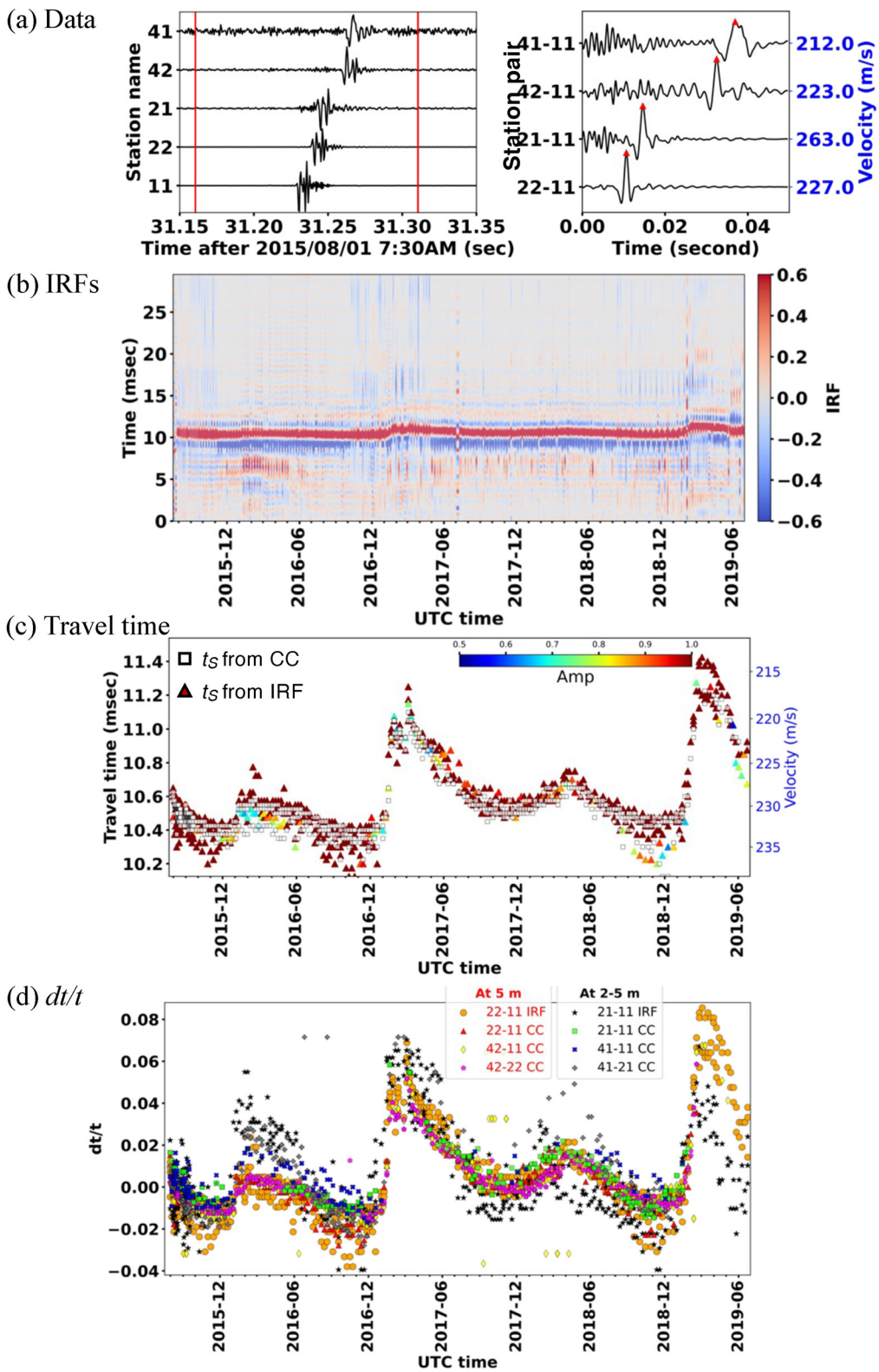

Figure 3. Cross-hole experiment data analysis: (a) Waveforms from a cross-hole experiment with impulse response functions (IRFs) calculated in the 0.15-s-long window (between red vertical lines). (b) All IRFs from station pair 22-11. (c) t_S from 22-11 estimated via IRF (triangles) and cross-correlation (white squares). Triangle colors represent peak amplitudes. (d). *dt/t* from all station pairs. Warm and cool colors illustrate results at 5 m and 2–5 m, respectively.

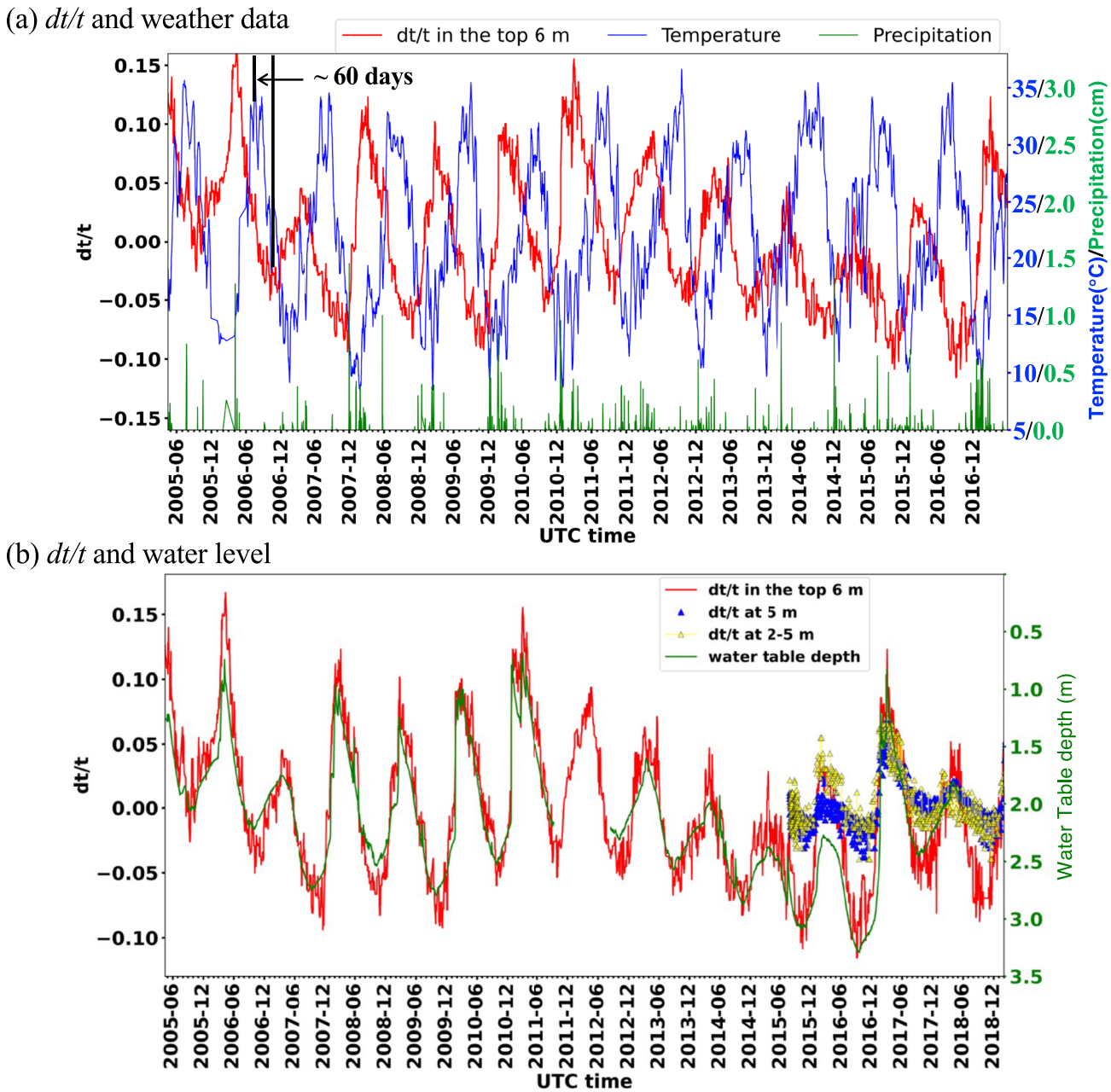

Figure 4. (a) Comparison between the *dt/t* curves averaged in the top 6 m (red curve; same as Figure 2c) and precipitation (green lines) and surface temperature (blue curve) recordings at the San Jacinto weather station. (b) Water table depth (green curve) and *dt/t* curves from impulse response function analyses of earthquakes and cross-hole experiment data.

table (fluctuating around 2 m in depth), and vice versa. During the winter storms in early 2017 that brought the water table height above 2 m the *dt/t* increased by almost 5%, while in the drought years between 2012 and 2016 a long-term decrease of the water table correlates well with a long-term decreasing trend of *dt/t*. During the analyzed period, all stations used in this work are below the water table, except 21 and 41 (2 m deep) that are occasionally above it. This may contribute to the scatterings of *dt/t* values at 2–5 m and slight discrepancies between *dt/t* values at 5 m and 2–5 m.

The *dt/t* variation in the top 6 m is almost linearly related to the water table height. The soil moisture effect is not visible likely because of the high-saturation level of the soil caused by the near-surface water table at the site. This suggests that the V_S changes in the shallow materials are induced primarily by fluid pressure variations

due to the change in the overlying water column height (Clements, 2021, and references therein). As the water level rises, fluid pressure reduces the effective stress in the sediments, decreasing the shear modulus more than it increases the mass density, and thus V_S decreases (e.g., Li et al., 2018; Mahmoodabadi & Bryson, 2021; West & Menke, 2000). The amount of V_S variation in response to pore pressure change highly depends on the soil properties (e.g., porosity) and drying/wetting state (e.g., Inci et al., 2003). Based on laboratory experiments (e.g., Dong & Lu, 2016), *Vs* variation of silt can range from 1,000 m/s when dry to tens of meters per second when fully saturated. Since the top 6 m is mainly composed of alluvial soils with a range of grain size from sands to clays (Figure 1b), the observed velocity variations at ~150–250 m/s (Figure 2b) may imply ~5–10% volumetric water content change.

Considering the correlation of *dt*/*t* and water table depth curves in both annual and decadal time scales, the water level change is the major driving mechanism for the observed variations. However, thermoelastic strain at shallow materials (e.g., top 1 m) can also contribute to the observed *dt*/*t* and velocity changes (e.g., Oakley et al., 2021; Qiu et al., 2020). The subsurface variations caused by seasonal thermoelastic strain are delayed by 2–3 months relative to the surface temperature (e.g., Ben-Zion & Leary, 1986; Berger, 1975). This phase delay is similar to the phase delay between the observed *dt*/*t* and the temperature at GVDA, so the thermoelastic strain may slightly increase the *dt*/*t* variation induced by water level changes. We note that temperature variations and thermoelastic strain can also affect the moisture level at subsurface locations, thus also contributing to the effects of fluid.

Compared with the 25% *dt*/*t* variations in the top 6 m, the *dt*/*t* over 2–5 m only shows 10% variations. The differences could be caused by two mechanisms. First, the V_S change is expected to decrease with depth, since shallow materials are weaker, are under lower normal stress, and have higher thermoelastic strain compared with deeper materials. Second, the different dominant frequency bands used for the analysis in the top 6 m (1–30 Hz) and at 2–5 m (above 100 Hz) may resolve elastic properties of the near-surface materials over different scales (e.g., Pimienta et al., 2016; Sarout, 2012).

Monitoring studies have revealed widespread velocity changes in the subsurface (e.g., Lu & Ben-Zion, 2022; Niu et al., 2003; Wang et al., 2017; Wu et al., 2009). In particular, the correlation of subsurface velocity changes with underground water level has led to the growth of hydrological monitoring work using seismological tools (e.g., Mao et al., 2022; Rodríguez Tribaldos & Ajo-Franklin, 2021). Among these studies, observed velocity variations vary by three orders of magnitude from $\sim 10^{-4}$ to 10^{-1}, depending on the data and methods that are used, the site conditions, and the space-time domains over which the observations are averaged. A few other studies also show limited contribution of near-surface water level changes to the observed structural variation (Illien et al., 2021; Oakley et al., 2021), probably because of different site conditions, as well as different depth resolutions of the used data and method.

Our analysis based on data from densely deployed borehole instruments indicates V_S variations up to 25%, concentrated only in the top 6 m. Modeling results (Juarez & Ben-Zion, 2020; Yang et al., 2019) show that temporal changes in shallow structures may alter the wavefield over larger scales, and that changes in shallow materials may be improperly interpreted as variations in deep structure. In situ observations indicate that material variations tend to concentrate at shallow surface layers, while the bedrock below remains largely unchanged (e.g., Qin et al., 2020; Rubinstein & Beroza, 2005). This study reveals t_S variation up to ~0.01 s in the top 6 m, which can contribute ~0.1% apparent V_S variations if the reference travel time is 10 s, and thus may be improperly attributed to smaller variations in deeper structures. Monitoring methods with high spatio-temporal resolutions are required to correctly infer the amplitudes and locations of subsurface material changes.

5. Conclusions

Using high-quality borehole instruments at the GVDA site, we monitor near-surface material properties with high spatial resolution, and observe seasonal variations of near-surface materials with strong depth constraints. The results show seasonal V_S variations of up to ~10% in the depth range 2–5 m, 25% variations averaged in the top 6 m, and no changes below 6 m. The observed V_S variations are closely correlated with water level changes, implying that the major driving mechanism is pore pressure changes. Thermoelastic strain in near-surface materials, and coupling between changes of temperature and water content in the soil, can also contribute to the velocity variations. The observed large variations of seismic properties in the top few meters have implications

for environmental seismology, soil dynamics, and studies aiming to analyze temporal variations of properties at greater depths.

Data Availability Statement

All the analyzed seismic data are available at http://nees.ucsb.edu/data-portal (Station name: GVDA). The weather data is from the National Oceanic and Atmospheric Administration at https://www.ncdc.noaa.gov/cdo-web/datasets/GHCND/stations/GHCND:USC00047813/detail.

Acknowledgments
We acknowledge former UCSB students Robin Gee, Timothy Lamere and Kenneth S. Hudson who conducted preliminary analysis with the used data. We thank the Lake Hemet Municipal Water District that provides access to the monitoring site at Garner Valley, and especially Mr. Paul Hegarty for assistance with the facility operations and access to data from the Garner Valley field site. We also thank Guoliang Li (USC) and Congcong Yuan (Harvard) for useful discussions. The observations and analyses of geotechnical array data at UCSB are currently supported in part by the U.S. Department of Energy Office of Science (Awards DE-SC0020291 and DE-SC0016520), the U.S. Geological Survey Inter-governmental agency Personnel Agreement (IPA-Steidl), and the Pacific Gas & Electric Co. Geosciences division. Lei Qin is supported by the Fundamental Research Funds for the Central Universities, China University of Geosciences (Wuhan) (No. 106-162301212665). The manuscript benefited from useful comments by referees Hsin-Hua Huang and Luc Illien, Associate Editor Victor Tsai, and Editor Daoyuan Sun.

References

Aki, K., & Richards, P. G. (1980). *Quantitative seismology: Theory and methods*. W. H. Freeman and Co.

Archuleta, B. Y. R. J., Seale, H., Sangas, P. V., Baker, L. M., & Swain, S. T. (1992). Garner Valley downhole array of accelerometers: Instrumentation and preliminary data analysis. *Bulletin of the Seismological Society of America*, *82*(4), 1592–1621.

ASTM. (2014). *Standard test methods for crosshole seismic testing*. ASTM International. American Society for Testing and Materials. Retrieved from https://www.astm.org/d4428_d4428m-14.html

Batzle, M. L., Han, D. H., & Hofmann, R. (2006). Fluid mobility and frequency-dependent seismic velocity—Direct measurements. *Geophysics*, *71*(1), 1–9. https://doi.org/10.1190/1.2159053

Ben-Zion, Y., & Leary, P. (1986). Thermoelastic strain in a half-space covered by unconsolidated material. *Bulletin of the Seismological Society of America*, *76*(5), 1447–1460. https://doi.org/10.1785/bssa0760051447

Berger, J. (1975). A note on thermoelastic strains and tilts. *Journal of Geophysical Research*, *80*(2), 274–277. https://doi.org/10.1029/jb080i002p00274

Berryman, J. G., Berge, P. A., & Bonner, B. P. (2002). Estimating rock porosity and fluid saturation using only seismic velocities. *Geophysics*, *67*(2), 391–404. https://doi.org/10.1190/1.1468599

Biot, M. A. (1956a). Theory of elastic waves in a fluid-saturated porous solid. 1. Low frequency range. *Journal of the Acoustical Society of America*, *28*(2), 168–178. https://doi.org/10.1121/1.1908239

Biot, M. A. (1956b). Theory of propagation of elastic waves in a fluid-saturated porous solid II. Higher frequency range. *Journal of the Acoustical Society of America*, *28*(2), 179–191. https://doi.org/10.1121/1.1908241

Bonilla, L. F., Guéguen, P., & Ben-Zion, Y. (2019). Monitoring coseismic temporal changes of shallow material during strong ground motion with interferometry and autocorrelation. *Bulletin of the Seismological Society of America*, *109*(1), 187–198. https://doi.org/10.1785/0120180092

Bonilla, L. F., Steidl, J. H., Gariel, J. C., & Archuleta, R. J. (2002). Borehole response studies at the Garner Valley Downhole array, southern California. *Bulletin of the Seismological Society of America*, *92*(8), 3165–3179. https://doi.org/10.1785/0120010235

Boore, D. M., Thompson, E. M., & Cadet, H. (2011). Regional correlations of Vs30 and velocities averaged over depths less than and greater than 30 meters. *Bulletin of the Seismological Society of America*, *101*(6), 3046–3059. https://doi.org/10.1785/0120110071

Chandra, J., Guéguen, P., Steidl, J. H., & Bonilla, L. F. (2015). In situ assessment of the g–γ curve for characterizing the nonlinear response of soil: Application to the Garner Valley downhole array and the wildlife liquefaction array. *Bulletin of the Seismological Society of America*, *105*(2), 993–1010. https://doi.org/10.1785/0120140209

Cheng, A., & Toksöz, M. N. (1979). Inversion of seismic velocities for the pore aspect ratio spectrum of a rock. *Journal of Geophysical Research*, *84*(B13), 7533–7543. https://doi.org/10.1029/jb084ib13p07533

Clements, T. (2021). *Tracking groundwater with the ambient seismic field*. Doctoral Dissertation, Harvard University Graduate School of Arts and Sciences.

Clements, T., & Denolle, M. A. (2018). Tracking groundwater levels using the ambient seismic field. *Geophysical Research Letters*, *45*(13), 6459–6465. https://doi.org/10.1029/2018GL077706

Coutant, O. (1996). Observation of shallow anisotropy on local earthquake records at the Garner Valley, southern California, downhole array. *Bulletin of the Seismological Society of America*, *86*(2), 477–488.

De Landro, G., Amoroso, O., Russo, G., D'Agostino, N., Esposito, R., Emolo, A., & Zollo, A. (2022). Decade-long monitoring of seismic velocity changes at the Irpinia fault system (southern Italy) reveals pore pressure pulsations. *Scientific Reports*, *12*(1), 1–9. https://doi.org/10.1038/s41598-022-05365-x

Dong, Y., & Lu, N. (2016). Dependencies of shear wave velocity and shear modulus of soil on saturation. *Journal of Engineering Mechanics*, *142*(11), 04016083. https://doi.org/10.1061/(asce)em.1943-7889.0001147

Hoar, R. J. (1982). *Field measurement of seismic wave velocity and attenuation for dynamic analyses*. Ph.D. Dissertation, The University of Texas, (p. 479).

Hudson, K. S. (2017). *In situ observations of seismic wave propagation*. M. S. Thesis, (June).

Illien, L., Andermann, C., Sens-Schönfelder, C., Cook, K. L., Baidya, K. P., Adhikari, L. B., & Hovius, N. (2021). Subsurface moisture regulates Himalayan groundwater storage and discharge. *AGU Advances*, *2*(2), e2021AV000398. https://doi.org/10.1029/2021av000398

Inci, G., Yesiller, N., Kagawa, T., & Kagawa, T. (2003). Experimental investigation of dynamic response of compacted clayey soils. *Geotechnical Testing Journal*, *26*(2), 125. https://doi.org/10.1520/gtj11328j

Juarez, A., & Ben-Zion, Y. (2020). Effects of shallow-velocity reductions on 3D propagation of seismic waves. *Seismological Research Letters*, *91*(6), 3313–3322. https://doi.org/10.1785/0220200183

Kuster, G. T., & Toksöz, M. N. (1974). Velocity and attenuation of seismic waves in two-phase media: Part I theoretical formulations. *Geophysics*, *39*(5), 587–606. https://doi.org/10.1190/1.1440450

Lecocq, T., Longuevergne, L., Pedersen, H. A., Brenguier, F., & Stammler, K. (2017). Monitoring ground water storage at mesoscale using seismic noise: 30 years of continuous observation and thermo-elastic and hydrological modeling. *Scientific Reports*, *7*(1), 1–16. https://doi.org/10.1038/s41598-017-14468-9

Li, D., Wei, J., Di, B., Ding, P., Huang, S., & Shuai, D. (2018). Experimental study and theoretical interpretation of saturation effect on ultrasonic velocity in tight sandstones under different pressure conditions. *Geophysical Journal International*, *212*(3), 2226–2237. https://doi.org/10.1093/gji/ggx536

Lu, Y., & Ben-Zion, Y. (2022). Regional seismic velocity changes following the 2019 Mw7.1 ridgecrest California earthquake from autocorrelations and P/S converted waves. *Geophysical Journal International*, *228*(1), 620–630. https://doi.org/10.1093/gji/ggab350

Lu, Z., & Sabatier, J. M. (2009). Effects of soil water potential and moisture content on sound speed. *Soil Science Society of America Journal*, *73*(5), 1614–1625. https://doi.org/10.2136/sssaj2008.0073

Mahmoodabadi, M., & Bryson, L. S. (2021). Direct application of the soil–water characteristic curve to estimate the shear modulus of unsaturated soils. *International Journal of Geomechanics*, *21*(1), 04020243. https://doi.org/10.1061/(asce)gm.1943-5622.0001893

Mao, S., Lecointre, A., van der Hilst, R. D., & Campillo, M. (2022). Space-time monitoring of groundwater fluctuations with passive seismic interferometry. *Nature Communications*, *13*(1), 1–9. https://doi.org/10.1038/s41467-022-32194-3

Müller, T. M., Gurevich, B., & Lebedev, M. (2010). Seismic wave attenuation and dispersion resulting from wave-induced flow in porous rocks—A review. *Geophysics*, *75*(5), 75A147–75A164. https://doi.org/10.1190/1.3463417

Nakata, N., & Snieder, R. (2011). Near-surface weakening in Japan after the 2011 Tohoku-Oki earthquake. *Geophysical Research Letters*, *38*(17), L17302. https://doi.org/10.1029/2011GL048800

Nakata, N., & Snieder, R. (2012). Estimating near-surface shear wave velocities in Japan by applying seismic interferometry to KiK-net data. *Journal of Geophysical Research*, *117*(B1), B01308. https://doi.org/10.1029/2011JB008595

Niu, F., Silver, P. G., Nadeau, R. M., & McEvilly, T. V. (2003). Migration of seismic scatterers associated with the 1993 Parkfield aseismic transient event. *Nature*, *426*(6966), 544–548. https://doi.org/10.1038/nature02151

Nur, A., & Simmons, G. (1969). The effect of saturation on velocity in low porosity rocks. *Earth and Planetary Science Letters*, *7*(2), 183–193. https://doi.org/10.1016/0012-821X(69)90035-1

Oakley, D. O., Forsythe, B., Gu, X., Nyblade, A. A., & Brantley, S. L. (2021). Seismic ambient noise analyses reveal changing temperature and water signals to 10s of meters depth in the critical zone. *Journal of Geophysical Research: Earth Surface*, *126*(2), e2020JF005823. https://doi.org/10.1029/2020jf005823

Pimienta, L., Borgomano, J. V. M., Fortin, J., & Guéguen, Y. (2016). Modelling the drained/undrained transition: Effect of the measuring method and the boundary conditions. *Geophysical Prospecting*, *64*(4), 1098–1111. https://doi.org/10.1111/1365-2478.12390

Prieto, G. A., Parker, R. L., & Vernon, F. L. (2009). A Fortran 90 library for multitaper spectrum analysis. *Computers & Geosciences*, *35*(8), 1701–1710. https://doi.org/10.1016/j.cageo.2008.06.007

Qin, L., Ben-Zion, Y., Bonilla, L. F., & Steidl, J. H. (2020). Imaging and monitoring temporal changes of shallow seismic velocities at the Garner Valley near Anza, California, following the M7.2 2010 El Mayor-Cucapah earthquake. *Journal of Geophysical Research: Solid Earth*, *125*(1), 1–17. https://doi.org/10.1029/2019JB018070

Qiu, H., Hillers, G., & Ben-Zion, Y. (2020). Temporal changes of seismic velocities in the San Jacinto Fault zone associated with the 2016 Mw 5.2 Borrego Springs earthquake. *Geophysical Journal International*, *220*(3), 1536–1554. https://doi.org/10.1093/gji/ggz538

Qiu, H., Lin, F. C., & Ben-Zion, Y. (2019). Eikonal tomography of the southern California plate boundary region. *Journal of Geophysical Research: Solid Earth*, *124*(9), 9755–9779. https://doi.org/10.1029/2019jb017806

Qiu, T., Huang, Y., Guadalupe-Torres, Y., Baxter, C. D. P., & Fox, P. J. (2015). Effective soil density for small-strain shear waves in saturated granular materials. *Journal of Geotechnical and Geoenvironmental Engineering*, *141*(9), 04015036. https://doi.org/10.1061/(asce)gt.1943-5606.0001334

Rodríguez Tribaldos, V., & Ajo-Franklin, J. B. (2021). Aquifer monitoring using ambient seismic noise recorded with distributed acoustic sensing (DAS) deployed on dark fiber. *Journal of Geophysical Research: Solid Earth*, *126*(4), e2020JB021004. https://doi.org/10.1029/2020jb021004

Rubinstein, J. L., & Beroza, G. C. (2005). Depth constraints on nonlinear strong ground motion from the 2004 Parkfield earthquake. *Geophysical Research Letters*, *32*(14), 1–5. https://doi.org/10.1029/2005GL023189

Sarout, J. (2012). Impact of pore space topology on permeability, cut-off frequencies and validity of wave propagation theories. *Geophysical Journal International*, *189*(1), 481–492. https://doi.org/10.1111/j.1365-246x.2011.05329.x

Solazzi, S. G., Guarracino, L., Rubino, J. G., & Holliger, K. (2019). Saturation hysteresis effects on the seismic signatures of partially saturated heterogeneous porous rocks. *Journal of Geophysical Research: Solid Earth*, *124*(11), 11316–11335. https://doi.org/10.1029/2019JB017726

Steidl, J. H., Civilini, F., & Seale, S. (2014). What have we learned after a decade of experiments and monitoring at the NEES@UCSB permanently instrumented field sites? *Proceedings of the 10th National Conference in Earthquake Engineering*. https://doi.org/10.4231/D3J96097W

Steidl, J. H., Tumarkin, A. G., & Archuleta, R. J. (1996). What is a reference site? *Bulletin of the Seismological Society of America*, *86*(6), 1733–1748. https://doi.org/10.1007/s00163-017-0270-7

Tanimoto, T., & Wang, J. (2021). Incorporating wind information in the inversion of co-located pressure and seismic data for shallow elastic structure. *Journal of Geophysical Research: Solid Earth*, *126*(5), 1–18. https://doi.org/10.1029/2020JB021162

Theodulidis, N., Bard, P. Y., Archuleta, R., & Bouchon, M. (1996). Horizontal-to-vertical spectral ratio and geological conditions: The case of Garner Valley downhole array in southern California. *Bulletin of the Seismological Society of America*, *86*(2), 306–319. https://doi.org/10.1785/bssa0860020306

Thomson, D. J. (1982). Spectrum estimation and harmonic analysis. *Proceedings of the IEEE*, *70*(9), 1055–1096. https://doi.org/10.1109/proc.1982.12433

Uyanik, O., Ekinci, B., & Uyanik, N. A. (2013). Liquefaction analysis from seismic velocities and determination of lagoon limits Kumluca/Antalya example. *Journal of Applied Geophysics*, *95*, 90–103. https://doi.org/10.1016/j.jappgeo.2013.05.008

Wang, Q. Y., Brenguier, F., Campillo, M., Lecointre, A., Takeda, T., & Aoki, Y. (2017). Seasonal crustal seismic velocity changes throughout Japan. *Journal of Geophysical Research: Solid Earth*, *122*(10), 7987–8002. https://doi.org/10.1002/2017JB014307

West, M., & Menke, W. (2000). Fluid-induced changes in shear velocity from surface waves. In *13th EEGS symposium on the application of geophysics to engineering and environmental problems*. European Association of Geoscientists & Engineers.

Wu, C., Peng, Z., & Assimaki, D. (2009). Temporal changes in site response associated with the strong ground motion of the 2004 Mw 6.6 Mid-Niigata earthquake sequences in Japan. *Bulletin of the Seismological Society of America*, *99*(6), 3487–3895. https://doi.org/10.1785/0120090108

Wu, C., Peng, Z., & Ben-Zion, Y. (2010). Refined thresholds for non-linear ground motion and temporal changes of site response associated with medium-size earthquakes. *Geophysical Journal International*, *182*(3), 1567–1576. https://doi.org/10.1111/j.1365-246X.2010.04704.x

Yang, C., Li, G., Niu, F., & Ben-Zion, Y. (2019). Significant effects of shallow seismic and stress properties on phase velocities of Rayleigh waves up to 20s. *Pure and Applied Geophysics*, *176*(3), 1255–1267. https://doi.org/10.1007/s00024-018-2075-7

Youd, T. L., Bartholomew, H. A., & Proctor, J. S. (2004). Geotechnical logs and data from permanently instrumented field sites: Garner Valley downhole array (GVDA) and wildlife liquefaction array (WLA). *NEES@ UCSB internal report*.

Zigone, D., Ben-Zion, Y., Lehujeur, M., Campillo, M., Hillers, G., & Vernon, F. L. (2019). Imaging subsurface structures in the San Jacinto fault zone with high-frequency noise recorded by dense linear arrays. *Geophysical Journal International*, *217*(2), 879–893. https://doi.org/10.1093/gji/ggz069